Journal of Dermatological Science 63 (2011) 191–198

Contents lists available at ScienceDirect

Journal of Dermatological Science

journal homepage: www.elsevier.com/jds

Visualization and characterisation of defined hair follicle compartments by Fourier transform infrared (FTIR) imaging without labelling

Katherine Lau [a,b], Martin A.B. Hedegaard [c], Jennifer E. Kloepper [d], Ralf Paus [d,e], Bayden R. Wood [f], Volker Deckert [a,b,*]

[a] Institute of Physical Chemistry, Friedrich-Schiller University of Jena, 07743 Jena, Germany
[b] IPHT - Institute for Photonic Technology, Albert-Einstein-Str. 9, 07745 Jena, Germany
[c] Institute of Sensors, Signals and Electrotechnics, University of Southern Denmark, Campusvej 55, 5230 Odense M, Denmark
[d] Department of Dermatology, University of Lübeck, Ratzeburger Allee 160, 23538 Lübeck, Germany
[e] School of Translational Medicine, University of Manchester, Stopford Building, Oxford Road, Manchester M13 9PL, UK
[f] Centre for Biospectroscopy and School of Chemistry, Monash University, Victoria 3800, Australia

ARTICLE INFO

Article history:
Received 8 October 2010
Received in revised form 31 March 2011
Accepted 2 May 2011

Keywords:
Hair follicle
Cell classification
FT-IR
Spectroscopic imaging
Multivariate data analysis

ABSTRACT

Background: To visualise and characterise skin architecture, the tissue usually has to be destroyed and labelled.
Objectives: The use of Fourier transform infrared (FTIR) spectroscopy as a label-free, minimally sample destructive method to define hair follicular structure has been explored and demonstrated in this paper.
Methods: Human scalp skin cryosections were imaged using FTIR microscopy and the data was subsequently analysed with N-FINDR spectral unmixing algorithm.
Results: This resulted in an excellent distinction of known hair follicle tissue layers, which could be discerned based on their molecular structure.
Conclusion: The development of a minimally sample-destructive, label-free spectroscopy based technique that can differentiate layers of cells in the dermal papilla and connective tissue sheath in the mesenchyme of the hair follicle paves the way forward to identifying spectral markers important in wound healing and stem cell therapies.

1. Introduction

With the purpose of defining skin architecture and to characterise its appendages, the tissue usually has to be destroyed and labelled. For efficient use of such precious tissue samples, a label-free intravital method to image and characterise the skin and its appendages is required. The hair follicle is an optimal model system for exploring such label-free tissue/cell imaging and characterisation methods, as the hair follicle has a defined and well-characterised anatomical structure, and its cell types are well studied. Distinct cell types are clearly segregated in their respective compartments.

While staining the hair follicle sections with haematoxylin and eosin allows clear visualisation of the different follicular compartments (example in Fig. 1), it does not present their molecular features. Immunohistochemistry utilising specific antibodies permits the elucidation of information of specific proteins but prior knowledge is required and is a largely time-consuming and laborious process. Vibrational spectroscopy, on the contrary, allows the examination of molecular contents in a cell/tissue sample without labelling or prior knowledge of the cells [1].

Fourier transform infrared (FTIR) spectroscopy is a label-free technique that has been applied to the studies of different types of biological samples, to elucidate the molecular differences between cell and tissue types [2–7]. Since the infrared (IR) light does not damage samples and the IR absorbance directly correlates to the concentration of the functional group, not only is FTIR spectroscopy minimally sample-destructive and label-free. As the samples do not have to be labelled, they are reusable for further analyses. FTIR spectroscopy is moreover semi-quantitative; the intensity of the peaks correspond to the concentration of the vibrational groups, and highly sensitive to molecular changes in biological samples [2–7]; shifts in peak positions reflect changes in molecular structures of the vibrational groups. Analyses of spectra from biological samples can yield information on their contents in terms of proteins, nucleic acids, lipids and carbohydrates. Information on

* Corresponding author at: IPHT - Institute for Photonic Technology, Albert-Einstein-Str. 9, 07745 Jena, Germany. Tel.: +49 3641 206 113.
E-mail addresses: volker.deckert@ipht-jena.de, volker.deckert@uni-jena.de (V. Deckert).

0923-1811/$36.00
doi:10.1016/j.jdermsci.2011.05.002

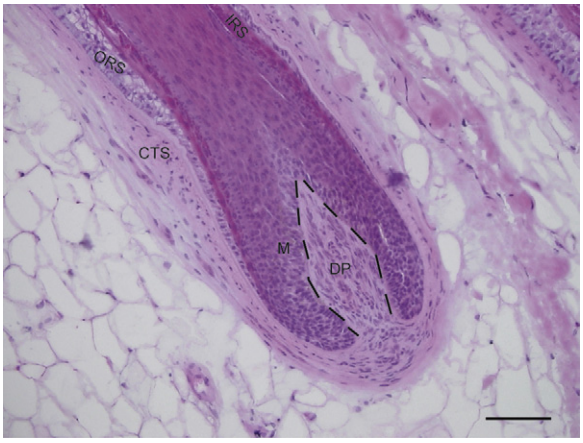

Fig. 1. (A) Microscopic image of an anagen VI human hair follicle (proximal part only) in a skin section, stained with haematoxylin and eosin. The staining helps define the hair follicular compartments but does not provide information on chemical composition. Scale bar: 100 μm. DP (dermal papilla, demarcated by the dotted white line), CTS (connective tissue sheath), IRS (inner root sheath), ORS (outer root sheath) and M (hair follicle matrix cells) belonging to the epithelium.

the conformation of lipids, proteins and nucleic acids can furthermore be extracted, by analysing their 'signature bands'. For example, the secondary structure of the proteins can be deduced by the position of maximum IR absorptions in the amide I and amide II bands [2,3]. By further use of multivariate data analysis, major differences in the 'finger print' region (around 1800–800 cm^{-1}) between samples can be revealed. Such combinations of techniques are extremely powerful for identifying 'abnormal' cells in a tissue sample, such as malignant cells [4–6] and for analysing the molecular differences between stem/progenitor cells and their more mature counterparts [2,7–9].

The aim of this work is to explore the potential use of FTIR spectroscopy to study single cells in the hair follicle, first by examining the employability of FTIR microspectroscopy and multivariate data analyses for discerning the tissue layers of the hair follicle, purely by means of their spectral differences. In this study we implemented N-FINDR spectral unmixing algorithm to achieve this [10]. Briefly, N-FINDR determines the most extreme or pure spectra within the data set, which are termed 'endmembers' (further elaborated in Section 2) [10]. Secondly, it was examined whether the locality of the so-called endmembers provided by this spectral unmixing algorithm matched the positions of the tissue layers in the visible image. Thirdly, the level of correlation between the spectral features and the biological features of each compartment was inspected.

The hair bulb is of particular interest since it contains the connective tissue sheath (CTS) and the dermal papilla (DP) where multipotent stem cells are located [11–15]. These cells had been shown to differentiate into adipocytes, osteocytes, chondrocytes, haematopoietic, neuronal and smooth muscle cells [13,16–20]. The distinct cell populations in different compartments – epithelial cells, CTS cells, DP cells and adipose tissue – further rendered the hair bulb suitable for addressing the above-mentioned questions we aimed to tackle.

Although previously a lateral cross-section of a hair follicle has been imaged using FTIR [21], it was neither characterised nor were the tissue compartments defined by the collected spectra. To our knowledge, this is the first report on using FTIR and multivariate analysis to discern tissue layers in a longitudinal hair bulb section. This report illustrates the biomolecular information extracted from the spectra of the individual clusters from the FTIR map, and discusses their biological significance in relationship to function. Four samples originating from the two different patients and different hair follicles were examined to confirm the reproducibility of the employed method.

2. Materials and methods

2.1. Sample origin

Human scalp skin was donated by routine facelift plastic surgery patients. All experiments were carried out according to the Helsinki guidelines, in compliance with national regulations for the experimental use of human material. The excised skin strips were transported in Williams E medium (Biochrom, Cambridge, UK) on ice and were subsequently cut into blocks before snap-freezing in liquid nitrogen and stored at −80 °C.

2.2. Skin section preparation

Snap-frozen skin strips were cryosectioned at 5 μm thickness and skin sections containing anagen VI hair follicles were mounted onto MirrIR low 'e' microscope slides (Kevley, OH, USA), which are coated with a silver reflective coating and further coated with tin oxide which minimizes the oxidation of the silver. The sections were fixed with 4% paraformaldehyde (in phosphate saline buffer) at room temperature for 20 min and washed 3 times with fresh reagent to remove the embedding compound and thus minimise spectral contamination.

2.3. Sample selection

FTIR measurements were performed on sections of hair follicle of which the shape and completeness were satisfactory. Four data sets (each data set acquired from a different section; Table 1) are presented in this paper, with data set 1 presented in the main text in details, and the rest are shown in the Supplementary Data. Data set 1 was acquired from a hair follicle from Patient A, while data sets 2–3 were from Patient B. Data sets 2 and 3 were acquired from different sections of the same hair follicle (approximately 10 μm apart).

2.4. FTIR measurement

The FTIR measurements were performed on a Perkin Elmer FTIR 2000 instrument in trans/reflection mode. Using Pemge30 software, a visible microscopy image was obtained to enable the specification of map area. A map region was established around the hair bulb (Fig. 2) of a 5 μm thick skin section, since we were particularly interested in the mesenchyme of the hair follicle. The interferograms were collected at a spectral resolution of 8 cm^{-1}. We applied an aperture size of 20 μm × 20 μm and a step size of 15 μm. During the map scan, 64 interferograms were co-added per spectrum, spanning the frequency range of 4000–700 cm^{-1}, and a background measurement was performed after every 5 spectra to minimize noise and water vapour signals.

2.5. Data analysis

The spectra were processed and analysed using MatLab software (Mathworks, USA). The spectra in data set 1 displayed Mie scattering artefacts [22], which severely affected the baseline in the 4000–2500 cm^{-1} region, consequently only the 1800–1000 cm^{-1} region was used in the ensuing analysis. The spectra were smoothed (13 points) and linear baseline corrected. Three regions in the map were omitted to remove artefacts from the evaluation (see blackened areas in Fig. 2) where perturbation due to liquid nitrogen refill was evident. N-FINDR, a spectral unmixing method similar to vertex component analysis (VCA) [23] and

Table 1
Detected peak positions and the corresponding vibrational groups.

Wave number value (cm^{-1})					Vibrational group (s)	Refs
Endmember						
1	2	3	4	5		
1744	1744	1744	1744	1744	Carbonyl ester (C=O) (lipid)	[30,31]
1648	1648	1648	1648	1648	Amide I (C=O) (C–N) ($N–R_2$) (protein)	[3,28,32]
1540	1532	1536	1532	1532	Amide II ($N–R_2$)+(C–N) (protein)	[3,32]
1452	1452	1448	1448	1448	CH_2 and CH_3 deformation vibrations due to lipid contribution	[3,32]
1376	1388	1388	1388	1384	Methyl	[32]
1284,1236	1284, 1240, 1204 *	1280,1232, 1204 *	1232	1276, 1228, 1204 *	Amide III C–N stretching, ($N–R_2$) and C–C stretching (*Collagen where triplet is present)	[3,32]
1156	1164	1160	1160	1160	C–OH in proteins C–O in carbohydrates	[51]
–	1084	1080	1080	1084	Phosphodiester $_{sym}PO_2^-$ stretching	[33,51]

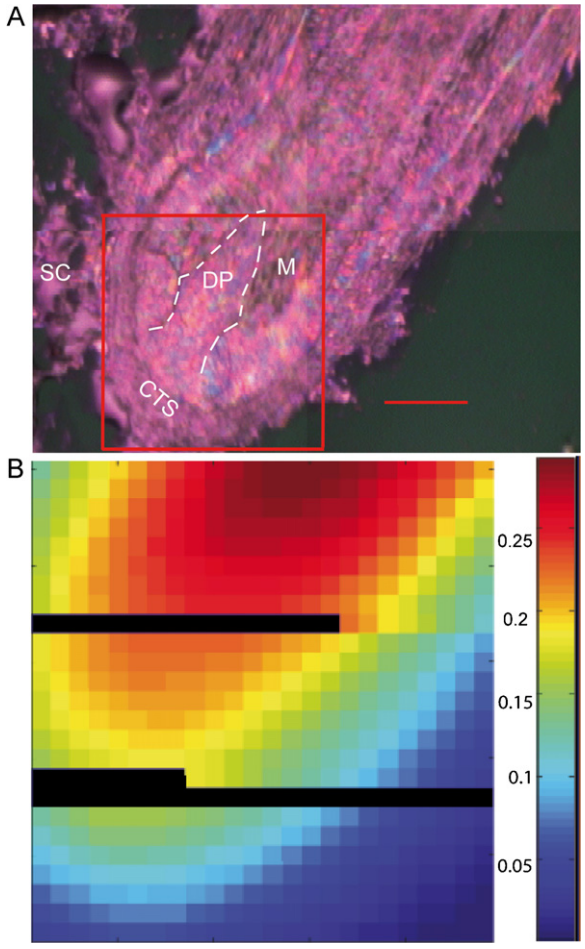

Fig. 2. (A) Microscopy image of an anagen VI human hair follicle in an unstained skin section, mounted on a Kevley low 'e' slide, is shown. The purple hue comes from the reflection of the thin silver coating. The red box indicates area of the hair bulb map scanned by FTIR. Scale bar: 100 μm. The tissue layers can be distinguished by eyes and are indicated by the labels SC (subcutis), DP (dermal papilla, demarcated by the dotted white line), CTS (connective tissue sheath), and M (hair follicle matrix cells) belonging to the epithelium. (B) Chemical image based on the integrated intensity of the band at 1648 cm^{-1} (amide I). (For interpretation of the references to color in this figure legend, the reader is referred to the web version of this article.)

iterated constrained endmembers (ICE) algorithm [24], was applied to the pre-processed data to extract five endmembers [10]. The algorithm assumes that "pure" spectra are present in the dataset and that they span the largest volume in the *n*-dimensional volume spanned by the spectral points of all the spectra present in the data set. Those assumed pure spectra are termed endmembers. In the implementation of N-FINDR a dimension reduction using principal component analysis (PCA) [25] was applied to the data set before calculating the largest volume. In the dimension reduced data set the positions of the "pure" spectra were found and the so-called endmembers extracted from the non-dimensionally reduced dataset. It must be noted that a pure spectrum does not refer to a pure compound. Rather, it can refer to a mixture of compounds, which can be detected in the sample. Ideally in our studies, the pure spectra refer to different tissue compartments.

All other spectra in the data set are then described as linear combinations of the found endmember spectra. This is achieved by a least squares fit with a non-negativity constraint of the endmembers to each spectrum in the data set. Each spectrum is then assigned an abundance value for each endmember that can be plotted in abundance maps. High abundances for one endmember in a spectrum indicate highly similar spectral features to the endmember and its spectrum. Overlapping of the components in the image map indicates a constitution of different spectral components in the spectra.

An evaluation was conducted to ensure the optimal number of endmembers was chosen. This was performed through PCA, which served to clarify the number of endmembers required to explain >99.95% of the spectral variance of the entire data set. To determine this number, the baseline corrected IR spectra (input spectra) were compared with the linear combination of the endmember spectra (output spectra) at the same point.

3. Results

3.1. Overall morphology and protein distribution according to IR spectra

The FTIR map scanned hair bulb is as shown in the visible image in Fig. 2A with a red box indicating the mapped area. The hair bulb map scanned area, to trained eyes, clearly contains the tissue layers dermal papilla (DP) which is in the centre, matrix cells surrounding the DP which belong to the epithelium, connective tissue sheath (CTS) which wraps around the hair follicle, separating the hair follicle from its surrounding adipose tissue, with the outermost

cuticle of the CTS intercalating with the adipose tissue. According to the chemical map plotted based on the integrated intensity of the band at 1648 cm^{-1} (Fig. 2B), which is assigned to amide I, protein is the most abundant in the centre where its locality corresponds to the DP. The intensity of amide I is graded by its colour showing downward gradation in the order of red, yellow, green and blue. A decrease in the intensity of amide I can be seen, from the centre outwards.

3.2. Specific FTIR spectra correspond to distinct hair follicle compartments as shown in data set 1

Using N-FINDR, five endmembers were determined for data set 1, three of which are presented in details (Fig. 3), with the rest briefly presented; further details can be found in Supp Data (Supp Fig. 1). Assignments of the IR absorption bands from which the chemical information can be interpreted, are tabulated in Table 1.

Endmember 1 has local abundances situated at the periphery of the hair bulb and has a low overall IR absorbance indicating the tissue is thin and porous where endmember 1 is present. The C=O band peaked at 1744 cm^{-1} assigned to the ester carbonyl group of fatty acids is very high relative to the absorbance displayed in the other endmembers, showing lipid as a major component in the periphery. Because there is also presence of proteins, indicated by the amide I and II bands, and amide III at 1236 and 1284 cm^{-1}, endmember 1 is likely to represent the spectra collected from the subcutis (SC) around the hair follicle, with some of the outer cuticle of CTS included.

Endmember 2 has local abundances in the upper centre of the map (Fig. 3), correlating to the location of DP. Its major bands peaked at 1644 and 1528 cm^{-1} (amide I and II) show high absorbance values compared to the amide I and II signals of the other endmembers (Fig. 3). The strong presence of amide I being the centre of the hair follicle is consistent with the chemical image based on the integrated intensity of amide I (Fig. 3B). The amide I band is a combination of three modes including $n(C{=}O) + n(C{-}N) + n(NH_2)$, while the amide II band which peaks at 1532 cm^{-1} is primarily composed of two modes $n(C{-}N) + n(NH_2)$, with a shoulder at 1516 cm^{-1}, as has been verified using the second derivative of the spectrum. The peaks in amide I with minima at 1644 and 1580 cm^{-1} indicate strong presence of β-sheet secondary structure protein, correlating with known intense immunostaining for anti-fibronectin found in the DP in an anagen follicle [26,27]. Fibronectin is predominantly of β-sheet secondary structure at room temperature [28,29]. The endmember exhibits a broad relative intense feature with a maxima at 1240 cm^{-1}, suggesting collagen and phosphate groups from nucleic acid remnants [5] are both present and the breadth of the peak is due to their overlapping in the spectrum [4]. Hence, endmember 2 is likely to represent spectra from the DP cells.

Endmember 5 has high abundances in the periphery of the mapped area and shows a relatively high amount of lipid, as indicated by the strong band at 1744 cm^{-1}, assigned to ester carbonyl mode of lipids [30,31]. It also naturally has a large amount of protein, as evinced by the intensity of the bands at 1648 and 1532 cm^{-1} [3,28,32]. The peaks at 1276, 1228 and 1204 cm^{-1} are typically present in collagen [32,33]. The weak profile of the collagen triplet between 1300–1200 cm^{-1} in endmember 5 suggests that collagen is not a major protein component. Endmember 5 comprises of lipids, proteins, collagen and carbohydrate (1156 cm^{-1}), and lies in the left periphery of the mapped area, strongly suggesting that endmember 5 represents CTS connected to the SC. The major difference between endmembers 1 and 5 lies in the proportion of proteins in the endmember and the overall IR absorbance.

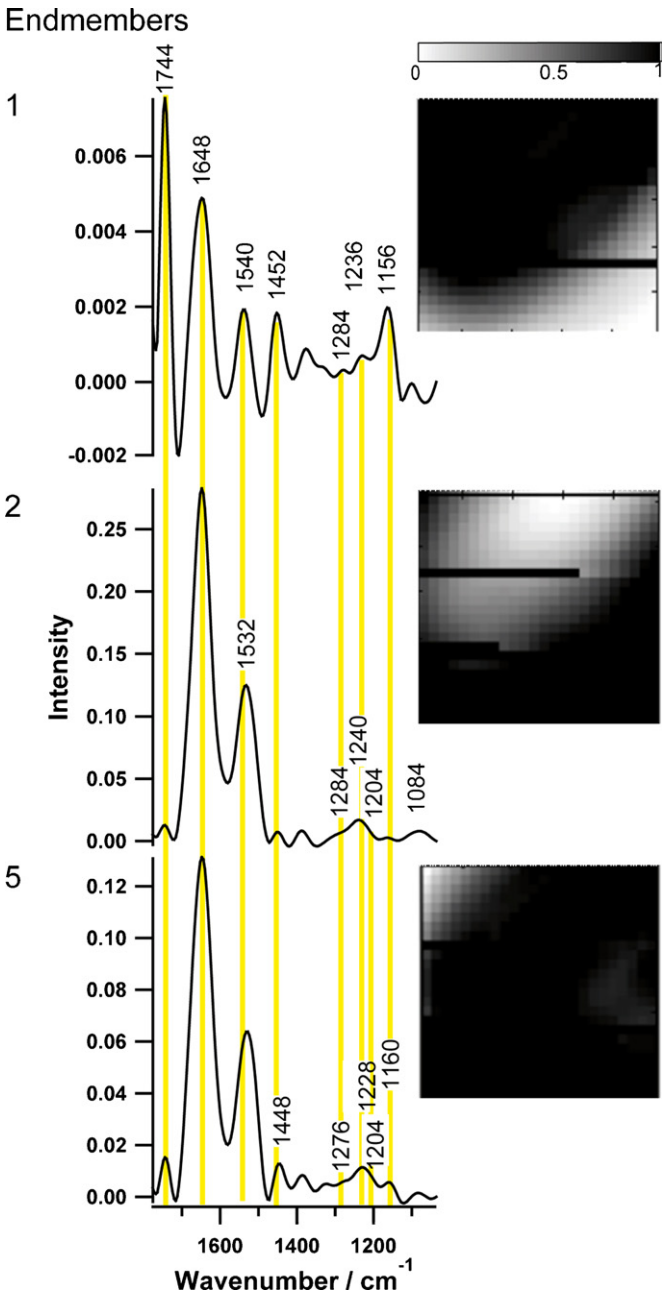

Fig. 3. The pure spectra of endmembers 1, 2 and 5 are shown in the left column, and the abundance maps of the endmembers shown in the right column. The spectra display infrared absorption intensity in arbitrary units against wavenumber values. The positions of the peak are as labelled and the vertical yellow lines serve to mark out bands assigned to the same vibrational groups. (For interpretation of the references to color in this figure legend, the reader is referred to the web version of this article.)

Position-wise, endmember 3 (Supp Fig. 1) being situated between endmember 1 (SC) and 2 (DP), is distinctive of CTS. This is supported by the strong presence of amide I and II and the so-called collagen triplet, less intense C=O band. Endmember 3 likely represents CTS proximal to the DP.

Endmember 4 is characterised by its high amide I to carbonyl ester ratio, which indicates that proteins are the main component in this endmember. In the second derivative spectrum its peak within the amide II band at 1512 cm^{-1} (data not shown) can be attributed to intracellular keratins, of which presence is known in the hair follicle epithelium [34,35]. Therefore, endmember 4 likely represents the hair follicle matrix cells of the epithelium.

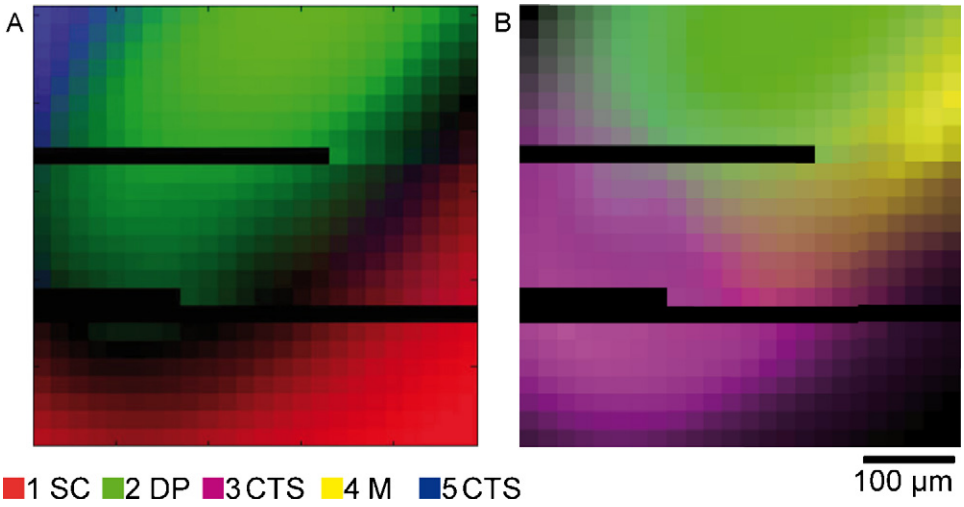

Fig. 4. (A) The abundance maps of endmembers 1 (red; SC), 2 (green; DP) and 5 (blue; CTS) are displayed on one map. The overlapping areas between blue and green indicate pixels with characteristics of both endmembers 2 (DP) and 5 (CTS) in their spectra. Overlapping is found neither between endmembers 1 (SC) and 2 (DP), nor 1 (SC) and 5 (CTS). (B) The abundance maps of endmember 2 (green; DP), 3 (lilac; CTS) and 4 (yellow; M) are plotted on the same map. Slight overlapping can be found between endmembers 2 and 3, as well as 2 and 4. SC, subcutis; DP, dermal papilla; CTS, connective tissue sheath; M, hair follicle matrix cells. (For interpretation of the references to color in this figure legend, the reader is referred to the web version of this article.)

3.3. N-FINDR abundance maps in relation to hair follicular anatomy

By assigning a colour to each endmember and showing their abundance distribution, a spatial presentation of endmembers was achieved (Fig. 4). The presentation of the abundance of endmembers 1 (SC), 2 (DP) and 5 (CTS) in Fig. 4A shows no overlapping between endmembers 1 (SC with some outer CTS cuticle), and endmember 2 (pure DP). A small degree of overlapping between endmembers 2 (DP) and 5 (CTS) exists, and does also between endmembers 1 (SC) and 3 (CTS) (Fig. 3B). The distribution of endmembers 3 (CTS) and 4 (epithelium) can also be seen in Fig. 4B. The brownish pixels correspond to overlapped endmembers. By displaying the abundance maps of endmembers 2 (DP), 3 (CTS) and 4 (epithelium), it can be clearly seen that endmember 4 (epithelium) is located in between (Fig. 3B). The spatial information of the endmembers relates to one another in such a way that they resemble the positions the tissue layers are found in the mapped hair bulb (Fig. 2A).

4. Discussion

To enable the study of cells in the hair follicle in a label-free and minimally sample-destructive manner, a method that permits the observation and identification of cells within the hair follicle was developed and demonstrated by FTIR mapping and N-FINDR. Without labelling, the chemical information of each layer was evidently extracted from the endmember spectra. The aperture size of 20 μm and interval of 15 μm provided a spatial resolution sufficiently small to differentiate between layers, yet large enough to produce good signal-to-noise ratios in the spectra. The parameters did not enable single cell lateral resolution, but as the aim of this work was to discern tissue compartments, higher resolution was in this case not sought.

4.1. Biological relevance of the N-FINDR results

The human anagen VI hair follicle is well extended into the SC and the hair follicle mesenchymal stem cells (MSCs) are known to differentiate into a number of lineages including adipocytes [13,16,18]; paraformaldehyde was thus chosen as a fixing agent to preserve the lipid features in our sample.

Our data show that the centre of the follicle is lipid poor and protein rich (see endmember 2, Fig. 3). Thus, our report is in line with a published study where FTIR spectroscopy imaging was applied on a skin tissue sample, in which a cross section of the hair follicle was captured [21].

By using a combination of FTIR spectroscopy and N-FINDR spectral unmixing analysis, the CTS and the DP could be differentiated as they express different endmembers. The literature has shown that CTS and DP fibroblasts contain different properties and functions (Table 2). For instance, the expression of cell surface markers differs; the protein expression of CD10 *in vivo* by CTS and the absence of which in the DP and the surrounding interfollicular dermis [36,37]. Functionality-wise, the DP cells (but not the CTS cells) produce and release anagen inductive signals such as WNT and bone morphogenic protein signalling molecules [38,39], and continue to stimulate hair growth by releasing signalling molecules such as insulin-like growth factor 1 and fibroblast growth factor 7 towards the matrix cells [40]. The FTIR data are therefore consistent as N-FINDR clearly separated the DP and the CTS into distinct entities; and have shown the highest protein level was found in the DP among the tissue layers, consistent with its role of actively synthesising signalling molecules essentially composed of protein.

The CTS is composed of fibroblasts and a collagenous matrix characteristic of connective tissues. It functions as a tissue sheath surrounding the hair follicle and separates the follicle from its neighbouring SC. Due to the connection of the CTS outer cuticle to the adipose of the SC, the spectra obtained from the region (endmembers 1 and 5) reflected a high lipids level as expected. The MSCs in the CTS have already been shown to be able to differentiate into multi-lineages including adipocytes *in vitro* [13]. The increase in lipid contents towards the outer layers of the CTS as reflected by our spectra, supports a published hypothesis which suggested that the hair follicle mesenchyme was a source of pre-adipocytes that could be found distributed around the hair follicle, both during hair follicle development in foetal/neonatal animals, as well as in adults [41]. It was deemed highly conceivable that the pre-adipocytes contributing towards the perifollicular subcutaneous adipose tissue originate from the hair follicle mesenchyme and this phenomenon may well continue into adulthood [41]; our data is clearly in agreement with this hypothesis.

Table 2
The properties of DP cells, in comparison to CTS cells, are tabulated below.

Only found in DP cells	Found in both CTS and DP cells
In utero (originally present as a condensed body of mesenchymal cells) DP cells induce hair follicle placode development into hair germ during hair follicle formation in foetal and neonatal skin, as well as in adult (murine) repaired wounds[52]	DP and trichogenic CTS cells *in vivo* have been shown to upregulate alkaline phosphatase protein and smooth muscle actin expression [53–56]
DP cells signal towards the hair follicle epithelium before a catagen (regression phase) to anagen (growth phase) transition is initiated [40,45]	Cultured DP and CTS cells both spontaneously aggregated and had similar morphology [56,57]
	Both isolated DPs and CTS were able o induce *de novo* folliculogenesis when implanted into sub-epidermal skin [58–60]

According to the immunohistochemistry results in the literature, the DP should contain an ample amount of collagen in its extracellular matrix [26,27,42–44]. The reason the collagen triplet in endmember 2 is not as prominent as that in endmember 4 (CTS) may be attributed to the presence of phosphate groups from nucleic acid remnants and lipids [4], broadening what normally should appear as a triplet. Nevertheless, the peak is 1240 cm^{-1} centred, where the maxima of the collagen triplet lies [32], and is a clear indication of presence of both collagen and nucleic acids, reflecting the high level of transcription. The high level of transcription is in line with the knowledge of DP being an actively signalling centre [40,45].

4.2. Suitability of using N-FINDR on hair follicle spectra

The N-FINDR abundance maps exhibit a transition of characteristics between different endmembers in the hair bulb. Due to the aperture size and the step size, it is inevitable that some spectra consist of absorbance from cells in adjacent layers. Although this could be thought of an instrumental limitation since reducing the aperture size would also decrease the IR light reaching the sample, resulting in a lower signal-to-noise ratio, the results also reflect the transitional nature of tissue layers. For instance, where both DP and CTS overlap (Fig. 4B), it is clear that the contributions of either endmember are low, indicating this transitional zone is the inter-DP/CTS boundary. While DP and CTS fibroblasts are distinguishable from each other, they are also inter-exchangeable [46,47] and CTS is capable of regenerating a DP [48,49]; thus some fibroblasts may display both DP and CTS characters. Transitioning between endmembers 3 and 5 is as predicted, as the CTS gradually becomes more cuticle-like and interlaces with the surrounding SC. For the mixing of endmember 4 (epithelium) with endmembers 2 and 3 (DP and mesenchyme), although distinct boundaries between epithelial and mesenchymal layers can usually be drawn, mesenchymal cells have been reported to interact with the follicular epithelial cells [26]. Such interaction is mediated via direct cell contact through a punctuated basement membrane, and by extending cytoplasmic processes of mesenchymal cells into the epithelial layer [26]. Moreover, CTS cells are known to penetrate the glassy membrane between the outer root sheath of the epithelium and the CTS to initiate cell contact with the epithelial cells at the beginning of anagen [26].

While endmember extraction methods effectively show where spectra display mixed spectral characteristics and to what extent, analytical tools such as unsupervised hierarchical clustering analysis and K-means clustering are also powerful [4,50]. However, since these clustering methods result in hard borders, and our spectra were recorded using aperture larger than an average cell size, N-FINDR was chosen for a more realistic interpretation.

By applying N-FINDR to data sets acquired from different hair follicles from two patients, as well as two sections from the same hair follicle (see Supp. Data), the reproducibility of N-FINDR is evidently demonstrated. Due to the different shapes and orientation of the hair follicles within the skin, no two hair follicles look the same. The abundance maps of the endmembers in different data sets are thus not identical. Nevertheless, the major tissue layers were discernible by the FTIR spectral analysis.

4.3. Perspectives for the use of FTIR microspectroscopy in the hair biology field

Having proven the employability of FTIR microspectroscopy to distinguishing tissue types, the next immediate aim is to identify and characterise single cells, based on their molecular fingerprints, by improving the spatial resolution. This will be realised by the help of focal plane array-, attenuated total reflection- and Synchrotron-FTIR technologies, as well as Raman spectroscopy. Future work points towards the identification of hair follicle stem cells with FTIR spectroscopy and depicting their participation in dermal wound healing.

5. Conclusions

The main purpose of this study was to demonstrate the feasibility of applying FTIR spectroscopy and spectral unmixing algorithms to tell apart major tissue layers in the hair follicle. Having proven this applicability, we are confident that increases in resolution will allow more minor details to be distinguished. The potentials of vibrational spectroscopy for examining molecular changes in the hair follicle have hereby been demonstrated and can be applied in the future to an array of studies.

FTIR microspectroscopy and multivariate analysis have been successfully applied to mapping human anagen VI hair follicle end bulbs. To the best of our knowledge, this report demonstrates for the first time the applicability of FTIR spectroscopy to discerning the follicular tissue layers, based on their spectral variation, which can be molecularly assigned. Thus, the molecular information of the individual tissue layers can be simultaneously extracted directly. By comparing the spectral features to the known biological characteristics, the assignment of the clusters to the tissue layers was confirmed. Though possible for visualising the tissue layers, microscopy alone can neither directly elucidate molecular information (unless the samples are stained), nor provide a quantification of compounds. FTIR microspectroscopy, on the other hand, can be used as a minimally sample-destructive, non-labour intensive and semi-quantitative method.

Acknowledgments

The Perkin Elmer spectrometer was kindly provided by Dr. Michael Heise of ISAS Dortmund and generous help had been given by his group members. The advice from Dr. Melissa Mariani on spectral data analysis is highly appreciated. Financial support was provided by the Federal Ministry of Education and Research (BMBF) through the project ´Markerfreie Zelldiagnostik mit Nanometerauflösung´ (0312032B), Germany and the Alexander von Humboldt Foundation. Dr. Bayden Wood is supported by an Australian Research Council Discovery grant.

Appendix A. Supplementary data

Supplementary data associated with this article can be found, in the online version, at doi:10.1016/j.jdermsci.2011.05.002.

References

[1] Hedegaard M, Krafft C, Ditzel HJ, Johansen LE, Hassing S, Popp J. Discriminating isogenic cancer cells and identifying altered unsaturated fatty acid content as associated with metastasis status, using K-means clustering and partial least squares-discriminant analysis of Raman maps. Anal Chem 2010.

[2] Ami D, Neri T, Natalello A, Mereghetti P, Doglia SM, Zanoni M, et al. Embryonic stem cell differentiation studied by FT-IR spectroscopy Biochimica et Biophysica Acta (BBA). Mol Cell Res 2008;1783:98–106.

[3] Babrah J, McCarthy K, Lush RJ, Rye AD, Bessant C, Stone N. Fourier transform infrared spectroscopic studies of T-cell lymphoma, B-cell lymphoid and myeloid leukaemia cell lines. Analyst 2009;134:763–8.

[4] Wood BR, Chiriboga L, Yee H, Quinn MA, McNaughton D, Diem M. Fourier transform infrared (FTIR) spectral mapping of the cervical transformation zone, and dysplastic squamous epithelium. Gynecol Oncol 2004;93:59.

[5] Hammody Z, Argov S, Sahu RK, Cagnano E, Moreha R, Mordechai S. Distinction of malignant melanoma and epidermis using IR micro-spectroscopy and statistical methods. Analyst 2008;133:372–8.

[6] Baker MJ, Gazi E, Brown MD, Shanks JH, Clarke NW, Gardner P. Investigating FTIR based histopathology for the diagnosis of prostate cancer. J Biophotonic 2009;2:104–13.

[7] Walsh MJ, Fellous TG, Hammiche A, Lin W-R, Fullwood NJ, Grude O, et al. Fourier transform infrared microspectroscopy identifies symmetric po formula modifications as a marker of the putative stem cell region of human intestinal crypts. Stem Cells 2008;26:108–18.

[8] Walsh MJ, Hammiche A, Fellous TG, Nicholson JM, Cotte M, Susini J, et al. Tracking the cell hierarchy in the human intestine using biochemical signatures derived by mid-infrared microspectroscopy. Stem Cell Res 2009;3:15–27.

[9] Krafft C, Salzer R, Seitz S, Ern C, Schieker M. Differentiation of individual human mesenchymal stem cells probed by FTIR microscopic imaging. Analyst 2007;132:647–53.

[10] Winter ME. A proof of the N-FINDR algorithm for the automated detection of endmembers in a hyperspectral image. Proc SPIE 2004;5425:31–41.

[11] Jahoda CAB, Reynolds AJ. Hair follicle dermal sheath cells: unsung participants in wound healing. Lancet 2001;358:1445–8.

[12] Gharzi A, Reynolds AJ, Jahoda CAB. Plasticity of hair follicle dermal cells in wound healing and induction. Exp Dermatol 2003;12:126–36.

[13] Jahoda CAB, Whitehouse CJ, Reynolds AJ, Hole N. Hair follicle dermal cells differentiate into adipogenic and osteogenic lineages. Exp Dermatol (Blackwell Synergy) 2003;849–59.

[14] Richardson G, Arnott E, Whitehouse C, Lawrence C, Reynolds A, Hole N, et al. Plasticity of rodent and human hair follicle dermal cells: implications for cell therapy and tissue engineering. J Investig Dermatol Symp Proc 2005;10:180–3.

[15] Lau K, Paus R, Tiede S, Day P, Bayat A. Exploring the role of stem cells in cutaneous wound healing. Exp Dermatol 2009;18:921–33.

[16] Kiseleva EV, Chermnykh ES, Vorotelyak EA, Volozhin AI, Vasiliev AV, Terskikh VV. Differentiation capacity of stromal fibroblast-like cells from human bone marrow, adipose tissue, hair follicle dermal papilla and derma. Cell Tissue Biol 2009;3:42–9.

[17] Lako M, Armstrong L, Cairns P, Harris S, Hole N, Jahoda C. Hair follicle dermal cells repopulate the mouse haematopoietic system. J Cell Sci 2002;115:3967–74.

[18] Hoogduijn MJ, Gorjup E, Genever PG. Comparative characterization of hair follicle dermal stem cells and bone marrow mesenchymal stem cells. Stem Cells Dev 2006;15:49–60.

[19] Liu JY, Peng HF, Gopinath S, Tian J, Andreadis ST. Derivation of functional smooth muscle cells from multipotent human hair follicle mesenchymal stem cells. Tissue Eng A 2010;16:2553–64.

[20] Kruse C, Bodo E, Petschnik AE, Danner S, Tiede S, Paus R. Towards the development of a pragmatic technique for isolating and differentiating nestin-positive cells from human scalp skin into neuronal and glial cell populations: generating neurons from human skin? Exp Dermatol 2006;15:794–800.

[21] Mendelsohn R, Chen H-C, Rerek ME, Moore DJ. Infrared microspectroscopic imaging maps the spatial distribution of exogenous molecules in skin. J Biomed Opt 2003;8:185–90.

[22] Bassan P, Byrne HJ, Bonnier F, Lee J, Dumas P, Gardner P. Resonant Mie scattering in infrared spectroscopy of biological materials—understanding the 'dispersion artefact'. Analyst 2009;134:1586–93.

[23] Nascimento JMP, Dias JMB. Vertex component analysis: a fast algorithm to extract endmembers spectra from hyperspectral data. pattern recognition and image analysis. Berlin/Heidelberg: Springer; 2003. p. 626–35.

[24] Berman M, Phatak A, Lagerstrom R, Wood BR. ICE: a new method for the multivariate curve resolution of hyperspectral images. J Chemometr 2009;23:101–16.

[25] Wold S. Pattern recognition by means of disjoint principal component models. Pattern Recogn 1976;8:127–39.

[26] Jahoda CA, Mauger A, Bard S, Sengel P. Changes in fibronectin, laminin and type IV collagen distribution relate to basement membrane restructuring during the rat vibrassa follicle hair growth cycle. J Anat 1992;181:47–60.

[27] Couchman J, Gibson W. Expression of basement membrane components through morphological changes in the hair growth cycle. Dev Biol 1985;108:290–8.

[28] Pauthe E, Pelta J, Patel S, Lairez D, Goubard F. Temperature-induced [beta]-aggregation of fibronectin in aqueous solution. Biochim Biophys Acta 2002;1597:12–21.

[29] Brumfeld V, Werber MM. Studies on fibronectin and its domains. II. Secondary structure and spatial configuration of fibronectin and of its domains. Arch Biochem Biophys 1993;302:134–43.

[30] Li Y-Z, Quan Y-S, Zang L, Jin MN, Kamiyama F, Katsumi H, et al. Transdermal delivery of insulin using trypsin as a biochemical enhancer. Biol Pharm Bull 2008;31:1574–9.

[31] Pillai O, Panchagnula R. Transdermal iontophoresis of insulin. Skin Pharmacol Physiol 2004;17:289–97.

[32] Potter K, Kidder L, Levin I, Lewis E, Spencer R. Imaging of collagen and proteoglycan in cartilage sections using fourier transform infrared spectral imaging. Arthritis Rheum 2001;44:846–55.

[33] Kohler A, Bertrand D, Martens H, Hannesson K, Kirschner C, Ofstad R. Multivariate image analysis of a set of FTIR microspectroscopy images of aged bovine muscle tissue combining image and design information. Anal Bioanal Chem 2007;389:1143–53.

[34] Heid H, Moll I, Franke W. Patterns of expression of trichocytic and epithelial cytokeratins in mammalian tissues. I. Human and bovine hair follicles. Differentiation 1988;137:137–57.

[35] Coulombe PA, Kopan R, Fuchs E. Expression of keratin K14 in the epidermis and hair follicle: insights into complex programs of differentiation. J Cell Biol 1989;109:2295–312.

[36] Poblet E, Jiminez J. CD10 and CD34 in fetal and adult human hair follicles: dynamic changes in their immunohistochemical expression during embryogenesis and hair cycling. Br J Dermatol 2008;159:646–52.

[37] Lee K, Choi Y, Kim W, Lee J, Yang J, Lee E, et al. CD10 is expressed in dermal sheath cells of the hair follicles in human scalp. Br J Dermatol 2006;155:841–65.

[38] Blanpain C, Fuchs E. Epidermal homeostasis: a balancing act of stem cells in the skin. Nat Rev Mol Cell Biol 2009;10:207–17.

[39] Rendl M, Polak L, Fuchs E. BMP signaling in dermal papilla cells is required for their hair follicle-inductive properties. Genes Dev 2008;22:543–57.

[40] Paus R, Cotsarelis G. The biology of hair follicles. N Engl J Med 1999;341:491–7.

[41] Wojciechowicz K, Markiewicz E, Jahoda C. C/EBP03B1: identifies differentiating preadipocytes around hair follicles in foetal and neonatal rat and mouse skin. Exp Dermatol 2008;17:675–80.

[42] Couchman JR. Rat hair follicle dermal papillae have an extracellular matrix containing basement membrane components. J Invest Dermatol 1986;87:762–7.

[43] Joubeh S, Mori O, Hashimoto T. Immunofluorescence analysis of the basement membrane zone components in human anagen hair follicles. Exp Dermatol 2003;12:365–70.

[44] Messenger A, Elliott K, Temple A, Randall V. Expression of basement membrane proteins and interstitial collagens in dermal papillae of human hair follicles. J Invest Dermatol 1991;96:93–7.

[45] Paus R, Foitzik K. In search of the "hair cycle clock": a guided tour. Differentiation 2004;72:489–511.

[46] Tobin D, Gunin A, Magerl M, Handijski B, Paus R. Plasticity and cytokinetic dynamics of the hair follicle mesenchyme during the hair growth cycle: implications for growth control and hair follicle transformations. J Investig Dermatol Symp Proc 2003;8.

[47] Chi WY, Enshell-Seijffers D, Morgan BA. De novo production of dermal papilla cells during the anagen phase of the hair cycle. J Invest Dermatol 2010.

[48] Oliver RF. Histological studies of whisker regeneration in the hooded rat. J Embryol Exp Morph 1966;16:231–44.

[49] Horne KA, Jahoda CAB. Restoration of hair growth by surgical implantation of follicular dermal sheath. Development 1992;116:563–71.

[50] Krafft C, Steiner G, Beleites C, Salzer R. Disease recognition by infrared and Raman spectroscopy. J Biophotonic 2009;2:13–28.

[51] Wong PTT, Wong RK, Caputo TA, Godwin TA, Rigas B. Infrared spectroscopy of exfoliated human cervical cells: evidence of extensive structural changes during carcinogenesis. Proc Natl Acad Sci USA 1991;88:10988–92.

[52] Ito M, Yang Z, Andl T, Cui C, Kim N, Millar SE, et al. Wnt-dependent de novo hair follicle regeneration in adult mouse skin after wounding. Nature 2007;447:316–21.

[53] McElwee KJ, Kissling S, Wenzel E, Huth A, Hoffmann R. Cultured peribulbar dermal sheath cells can induce hair follicle development and contribute to the dermal sheath and dermal papilla. J Invest Dermatol 2003;121:1267–75.

[54] Handjiski BK, Eichmuller S, Hofmann U, Czarnetzki BM, Paus R. Alkaline phosphatase activity and localization during the murine hair cycle. Br J Dermatol 1994;131:303–10.

[55] Iida M, Ihara S, Matsuzaki T. Hair cycle-dependent changes of alkaline phosphatase activity in the mesenchyme and epithelium in mouse vibrissal follicles. Dev Growth Differ 2007;49:185–95.

[56] Jahoda CAB, Reynolds AJ, Chaponnier C, Forester JC, Gabbiani G. Smooth muscle α-actin is a marker for hair follicle dermis in vivo and in vitro. J Cell Sci 1991;99:627–36.

[57] Ohyama M, Zheng Y, Paus R, Stenn KS. The mesenchymal component of hair follicle neogenesis: background, methods and molecular characterization. Exp Dermatol 2009;19.
[58] Matsuzaki T, Yoshizato K. Role of hair papilla cells on induction and regeneration processes of hair follicles. Wound Repair Regen 1998;6:524–30.
[59] Reynolds AJ, Lawrence C, Cserhalmi-Friedman PB, Christiano AM, Jahoda CAB. Trans-gender induction of hair follicles. Nature 1999;402:33–4.
[60] Qiao J, Zawadzka A, Philips E, Turetsky A, Batchelor S, Peacock J, et al. Hair follicle neogenesis induced by cultured human scalp dermal papilla cells. Regen Med 2009;667–76.